Monomeric Zinc(II) Amide Complexes Supported by Bidentate, Benzannulated Phenanthridine Amido Ligands

Issiah B. Lozada, Talon Murray and David E. Herbert*

Department of Chemistry and the Manitoba Institute for Materials, University of Manitoba, Winnipeg, MB R3T 2N2, Canada

*david.herbert@umanitoba.ca

ABSTRACT

The first examples of homoleptic zinc amides (**1-Zn** and **2-Zn**) supported by chelating, benzannulated 4-aminophenanthridine ligands (**L1**, **L2**) are reported. The organometallic compounds were characterized fully both in solution (NMR, UV-Vis, electrochemistry, emission spectroscopy) and the solid-state (X-ray crystallography, elemental analysis). X-ray structural analysis reveals the Zn complexes are monomeric in the solid-state, with distorted sawhorse or distorted tetrahedral structures enforced by the coordination geometry of the deprotonated forms of the bidentate amido ligands **L1** (4-(*N*-phenylamine)-2-*tert*-butylphenanthridine) and **L2** (2,6-dimethyl-4-(*N*-phenylamine)phenanthridine). Cyclic voltammetry shows quasi-reversible oxidations on the electrochemical timescale, which density functional theory (DFT) assigns as arising from the highest occupied molecular orbital (HOMO) comprised largely of the nitrogen lone pair and occupied *N*-phenyl π-orbitals. Ligand substitution plays a role in the

reversibility of the observed oxidation. In comparison, the lowest unoccupied molecular orbitals (LUMOs) of **L1**, **L2**, **1-Zn** and **2-Zn** are based wholly on the phenanthridine moiety. This engenders the lowest energy absorptions of both the proligands and zinc complexes with ligand-to-ligand charge transfer (LLCT) character, confirmed by time-dependent DFT (TD-DFT) calculations. Both **L1** and **1-Zn** are emissive in solution, with considerable quenching of emission intensity in the zinc complex. In comparison, **L2** and **2-Zn** are non-emissive.

KEYWORDS

zinc amides; benzannulated N-heterocyclic ligands; phenanthridine; x-ray crystallography; cyclic voltammetry

1. INTRODUCTION

After a quiet period following the earliest report of their synthesis by Frankland[1], amide complexes of zinc[2] have since found application as inverse crown metalation reagents[3], transamination reagents[4], biomimetic model complexes[5], catalysts for enantioselective addition reactions[6] and lactide ring-opening polymerization[7], and as volatile dopant precursors for film preparation by chemical vapor deposition[8]. In this last respect, controlling nuclearity to ensure volatility with minimal steric protection is important[9]. While the nuclearity of homoleptic, low-coordinate Zn amide complexes is typically controlled by sterics[10], monomeric Zn(II) amides with relatively sterically unencumbered 8-amidoquinoline ligands have been reported (Figure 1, **Zn(^{q}NN^{H})$_2$**)[5a], with distorted tetrahedral structures comparable to Zn(II) amides supported by more sterically imposing 8-(trialkylsilyl)amidoquinoline ligands (**Zn(^{q}NN^{SiMe3})$_2$**)[11].

As part of our investigation into multidentate ligand frameworks containing π-extended *N*-heterocyclic rings[12], we have prepared 2-alkyl-4-(*N*-aryl)aminophenanthridines combining phenanthridine (3,4-benzoquinoline) and secondary amine moieties. Compared with quinoline and acridine, multidentate ligand frameworks introducing phenanthridine into the coordination sphere of metals are relatively rare. Examples include *tris*(4-phenanthridinolato) complexes of lithium[13] and aluminum[14], explored as emissive components of electroluminescent devices, and atropisomeric phosphinamine ligands (*R*) and (*S*)-6-(2'-diphenylphosphino-l'-naphthyl) phenanthridines applied in Pd-catalyzed allylic alkylation[15]. Re(I) complexes of *fac*-binding, tertiary bis(phenanthridinylmethyl)amines have also been investigated for fluorescence imaging of live cells[16]. We have recently reported the construction and coordination chemistry of

tridentate phenanthridinyl/quinolinyl amido ligands with Group 10 metal ions[12b]. To our knowledge, the coordination chemistry of secondary phenanthridinylamides with zinc has yet to be reported (e.g., **Zn(ᵖNN^{Ph})$_2$**). We were curious as to the ability of these π-extended analogs of (8-amino)quinolines[17] to support mononuclear zinc(II) ions, given the relative low steric encumbrance of site-selective benzannulation in phenanthridine (3,4-benzoquinoline) compared with acridine (2,3-benzoquinoline).

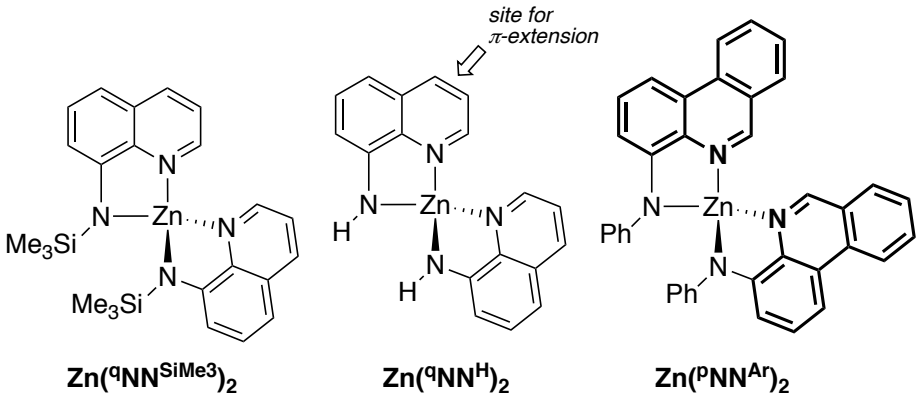

Figure 1. Mononuclear zinc amide complexes of amidoquinoline (**Zn(ᵠNN^{SiMe3})$_2$**[11] and **Zn(ᵠNN^{H})$_2$**[5a]) and amidophenanthridine **Zn(ᵖNN^{Ph})$_2$** (this work).

Herein, we report two such derivatives and demonstrate their ability to support tetracoordinate monomeric, homoleptic zinc(II) amide complexes. As phenanthridines and their metal complexes are known to exhibit rich and interesting trends in emission[12a,12c], we also report on the photophysical properties of the proligands and their zinc complexes. A quenching of ligand-based fluorescence is observed upon metalation with zinc.

2.1 MATERIALS AND METHODS

2.1 General Considerations

Air-sensitive manipulations were carried out either in a N_2-filled glove box or by using standard Schlenk techniques under Ar atmosphere. Bromobenzene (BDH), dppf (1,1'-diphenylphosphinoferrocene; Sigma Aldrich), $Pd_2(dba)_3$ (dba = dibenzylideneacetone; Sigma Aldrich), 2-formylphenyl boronic acid (Combi Blocks), Na_2CO_3 (Alfa Aesar), diethylzinc (15% w/w in hexanes; Alfa Aesar) were purchased and used without special purification. 4-amino-2-*tert*-butylphenanthridine and 4-amino-2,6-dimethylphenanthridine were prepared by analogy to published procedures.[12b] Solvents were dried and distilled by using appropriate drying agents and were oxygen free prior to use. NMR spectra were recorded on a Bruker Avance 300 MHz spectrometer. ^{1}H and $^{13}C\{^{1}H\}$ NMR spectra were referenced to residual solvent peaks[18] and assigned with the help of 2D ^{1}H-^{1}H COSY and ^{1}H-^{13}C HSQC/HMBC NMR spectra. Elemental analyses were performed at the University of Manitoba on a PerkinElmer EA2400 CHNS Analyzer.

Cyclic voltammetry was carried out using a CH Instruments 400C Series electrochemical analyzer/workstation in conjunction with a three-electrode cell. A BASi glassy carbon disk electrode (3.0 mm diameter) was used as the working electrode, a platinum wire the counter electrode, with a non-aqueous Ag/Ag^{+} quasi-reference electrode separated from the solution by a porous Teflon tip. All cyclic voltammetry (CV) measurements were conducted with 0.1 M nBu$_4$NPF$_6$ as the supporting electrolyte, at scan rates ranging from 50 mV/s to 800 mV/s. Ferrocene (FcH) was added to each solution as an internal reference, allowing the potentials to be referenced to the $FcH^{0/+}$ redox couple[19].

Diffraction data was collected from multi-faceted crystals of suitable size and quality selected from a representative sample of crystals of the same habit using an optical microscope. In each case, crystals were mounted on MiTiGen loops with data collection carried out in a cold stream of nitrogen (150 K; Bruker D8 QUEST ECO). All diffractometer manipulations were carried out using Bruker APEX3 software[20]. Structure solution and refinement was carried out using XS, XT and XL software, embedded within the Bruker SHELXTL suite[21]. For each structure, the absence of additional symmetry was confirmed using ADDSYM incorporated in the PLATON program[22]. CCDC Nos. 1868447-1868448 contain the supplementary crystallographic data for this paper. The data can be obtained free of charge from The Cambridge Crystallographic Data Centre via www.ccdc.cam.ac.uk/structures.

Solution samples for absorption and emission spectroscopy were prepared in a nitrogen-filled glovebox by dissolving the proligands or complexes in THF. A similar procedure was carried out for the protonated ligands outside the glovebox using distilled THF. The complexes were also tested for aggregation-induced emission (AIE) by dissolving the complexes in different mixtures of THF/pentane. The solutions were kept in 10 x 10 mm^2 quartz cuvettes, under inert atmosphere. Absorption spectra of the ligands and the complexes were recorded with a Cary 5000 UV-Vis NIR spectrophotometer. Emission spectra were recorded with a PTI QM30 fluorimeter (1 nm slit widths, λ_{exc} = 366 nm). Fluorescence quantum yields (ϕ_f) were measured using quinine sulfate as standard[23] and employing equation (1):

$$\Phi_S = \Phi_R \frac{A_R I_S n_S^2}{A_S I_R n_R^2} \qquad (1)$$

where Φ_R is the reference quantum yield, I is the integrated emission spectra, A is the absorbance at the excitation wavelength (λ_{exc} = 366 nm), and n is the solvent refractive index.

All calculations were performed using Gaussian 16, Rev. B.01[24]. Solvent effects, using THF, were modeled using a polarizable continuum model (IEFPCM)[25]. Structures of **L1** and **L2** were built using the Avogadro molecular editor and visualizer[26], and optimized with the MN15L functional[27] and def2-TZVP basis set[28]. **1-Zn** and **2-Zn** were optimized using the MN15L functional and the def2-SVP on the lighter elements and the SDD basis set[29] on Zn, starting from the crystal structure coordinates. Frequency calculations were subsequently performed at the same levels of theory to confirm the structures are at a minimum. Single point calculations, including TD-DFT, were performed on the optimized structures with the B3LYP functional on both the proligands and the complexes[30]. The def2-tzvp basis set was used on the proligands, while a split basis obtained from the EMSL basis set library[31] was used for the metal complexes, with the def2-SVPD basis set on the lighter elements[32] and the SDD basis set on zinc. TD-DFT analyses were performed with the GaussSum program[33] while orbital composition analyses were carried out using QMForge software[34]. Molecular orbitals were prepared using Avogadro[26].

2.2 Synthesis of Compounds

*2.2.1 Synthesis of 4-amino-2-tert-butylphenanthridine (**L1**)*

A thick-walled 100 mL Teflon-stoppered flask was charged with dppf (0.27 g, 0.49 mmol), $Pd_2(dba)_3$ (0.22 g, 0.24 mmol) and toluene (50 mL). 4-amino-2-*tert*-butylphenanthridine

(1.5 g, 6.0 mmol), bromobenzene (0.63 mL, 6.0 mmol), and NaO*t*Bu (1.20 g, 12.1 mmol) were added into the reaction vessel. The vessel was sealed and the solution was stirred vigorously for 24 h in a 155 °C oil bath. After careful cooling to room temperature, the resulting dark brown solution was filtered over Celite, passed through a silica plug and concentrated under reduced pressure at 50 °C to yield a spectroscopically pure, viscous, deep-brown oil which solidified upon standing. Yield = 1.6 g (80%). ^{1}H NMR ($CDCl_3$, 300 MHz, 25 °C): δ 9.13 (s, 1H; C_6H), 8.64 (d, J_{HH} = 8.2 Hz, 1H; $C_{10}H$), 8.29 (br s, 1H; N*H*), 8.05 (dd, J_{HH} = 0.8 Hz, 8.0 Hz, 1H; C_7H), 7.99 (d, J_{HH} = 1.9 Hz, 1H; C_1H), 7.85 (ddd, J_{HH} = 1.4 Hz, 6.9 Hz, 8.6 Hz, 1H; C_9H), 7.73 (d, J_{HH} = 1.9 Hz, 1H; C_3H), 7.70 (ddd, J_{HH} = 1.0 Hz, 6.8 Hz, 8.1 Hz, 1H; C_8H), 7.30-7.50 (m, 4H; $^{Ph}C_{12,13}H$), 7.03 (tt, J = 2.0 Hz, 6.6 Hz; $^{Ph}C_{14}H$), 1.47 ppm (s, 9H; $^{t\text{Bu}}C_{15}H$). $^{13}C\{^{1}H\}$ NMR ($CDCl_3$, 75 MHz, 25 °C): δ 150.75 (C_2), 149.85 (C_6), 142.57 (C_{11}), 140.35 (C_4), 133.10 (C_{6a}), 132.29 (C_{4b}), 130.74 (C_9), 129.51 ($C_{12/13}$), 128.83 (C_7), 127.27 (C_8), 126.99 (C_{6a}), 124.22 (C_{4a}), 122.41 (C_{10}), 121.74 (C_{14}), 119.52 ($C_{12/13}$), 108.39 (C_3), 107.62 (C_1), 35.63 (C_{16}), 31.62 ppm (C_{15}). UV-Vis (THF): λ (ε) 405 (sh), 355 (11 710 M^{-1} cm^{-1}), 309 nm (sh).

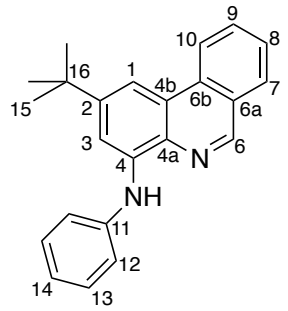

*2.2.2 Synthesis of 4-amino-(2,6-dimethyl)phenanthridine (**L2**)*

An identical procedure to the synthesis of **L1** was employed using dppf (0.31 g, 0.57 mmol), $Pd_2(dba)_3$ (0.25 g, 0.28 mmol) and toluene (50 mL), 4-amino-2,6-dimethylphenanthridine (1.5 g, 6.9 mmol), bromobenzene (0.73 mL, 6.9 mmol), and NaO^tBu (1.3 g, 14 mmol). Brown solid. Yield = 1.7 g (84%). ^1H NMR ($CDCl_3$, 300 MHz, 25 °C): δ 8.59 (d, J_{HH} = 8.2 Hz, 1H; $C_{10}H$), 8.38 (br s, 1H; N*H*), 8.20 (dd, J_{HH} = 0.5 Hz, 8.2 Hz, 1H; C_7H), 7.81 (ddd, J = 1.2 Hz, 6.8 Hz, 8.7 Hz, 1H; C_9H), 7.73 (br s, 1H; C_3H), 7.67 (ddd, J = 1.1 Hz, 6.8 Hz, 8.1 Hz, 1H; C_8H), 7.34-7.46 (m, 4H; $^{Ph}C_{12\text{-}13}H$), 7.04 (tt, J = 1.7 Hz, 6.8 Hz; $^{Ph}C_{14}H$), 3.03 (s, 3H; $C_{15}H$), 2.54 ppm (s, 3H; $C_{16}H$). $^{13}C\{^1H\}$ NMR ($CDCl_3$, 75 MHz, 25 °C): δ 154.89 (C_6), 142.42 (C_4), 140.23 (C_{4a}), 136.71 (C_{6a}), 132.70 C_{4b}), 131.12 (C_{11}), 130.14 (C_9), 129.43 (C_{12} or C_{13}), 127.10 (C_8), 126.55 (C_7), 126.39 (C_{6b}), 124.20 (C_2), 122.92 (C_{10}), 120.23 (C_{12} or C_{13}), 111.25 (C_1), 110.52 (C_3), 23.41 (C_{16}), 22.80 ppm (C_{15}). UV-Vis (THF): λ (ε) 402 (sh), 350 (10 000), 310 nm (17 870 M^{-1} cm^{-1}).

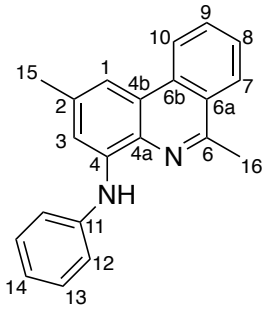

*2.2.3 Synthesis of bis(4-amido-2-tert-butylphenanthridine)zinc(II) (**1-Zn**)*

To a cooled solution of **L1** (0.101 g, 0.308 mmol) in hexanes (20 mL; -40 °C), diethylzinc (15% w/w in hexanes; 176 μL, 0.154 mmol) was added drop-wise and the mixture left stirring at room temperature for 12 h over which period, the solution colour changed from orange to deep red with formation of a red precipitate. The solvent was removed *in vacuo*

and the resulting residue was recrystallized in a mixture of hot (60 °C) hexanes/toluene (3:1) to give bright red crystals. Yield = 0.068 g (62%). ^{1}H NMR (C_6D_6, 300 MHz, 25 °C): δ 8.32 (d, J_{HH} = 8.4 Hz, 2H; $C_{10}H$), 8.25 (s, 2H; C_6H), 8.23 (d, J_{HH} = 1.7 Hz; C_1H), 7.69 (d, J = 1.6 Hz, 2H; C_3H), 7.30 (overlapped m, 2H; C_9H), 7.24 (m, 4H; $C_{12}H$, $C_{13}H$), 7.11 (overlapped m, 2H; C_7H), 7.04 (overlapped m, 2H; C_8H), 6.82 (tt, J_{HH} = 1.0, 7.3 Hz, 2H; $C_{14}H$), 1.46 ppm (s, 18H; $C_{15}H$). ^{13}C{^{1}H} NMR (C_6D_6, 75 MHz, 25 °C): δ 153.6 (C_2), 152.3 (C_{11}), 151.4 (C_4), 147.6 (C_6), 134.8 (C_{Ar}), 132.9 (C_{Ar}), 131.9 (C_9), 129.9 ($C_{13,}$ C_{15}), 129.6 (C_7), 126.9 (C_{Ar}), 126.7 (C_8), 126.1 (C_{Ar}), 123.2 ($C_{12,}$ C_{14}), 122.8 (C_{10}), 120.8 (C_{16}), 108.4 (C_1), 102.0 (C_3), 35.9 (C_{17}), 31.7 ppm (C_{18}). UV-Vis (THF): λ (ε) 515 (3 430), 392 (8 890), 362 (10 900 M^{-1} cm^{-1}), 328 nm (sh). Anal. Calc. for $C_{46}H_{42}N_4Zn$: C, 77.14; H, 5.91. Found: C, 77.20; H, 5.96.

Crystal structure data for **1-Zn**: X-ray quality crystals were grown as a diethylether solvate from diethylether/hexanes solution at -40 °C. Crystal structure parameters: $C_{54}H_{62}N_4O_2Zn$ 864.44 g/mol, triclinic, space group *P*-1; a = 10.9233(3) Å, b = 12.7212(4) Å, c = 17.6499(5) Å, α = 98.0488(15)°, β = 98.9851(15)°, γ = 105.0765(15)°, V = 2296.77(12) Å^3; Z = 2, ρ_{calcd} = 1.250 g cm^{-3}; crystal dimensions 0.402 x 0.287 x 0.152 mm; diffractometer Bruker D8 QUEST ECO CMOS; Mo K_α radiation, 150(2) K, θ_{max} = 30.595°; 90303 reflections, 14103 independent (R_{int} = 0.0450), direct methods; absorption coeff (μ = 0.580 mm^{-1}), absorption correction semi-empirical from equivalents (SADABS); refinement (against F_o^2) with SHELXTL V6.1, 560 parameters, 0 restraints, R_1 = 0.0536 ($I > 2\sigma$) and wR_2 = 0.1394 (all data), Goof = 1.037, residual electron density 1.385 /−1.410 e Å^{-3}.

*2.2.4 Synthesis of bis(4-amido-(2,6-dimethyl)phenanthridine)zinc(II) (**2-Zn**)*

A similar procedure to **1-Zn** was employed using **L2** (100 mg, 0.335 mmol), hexanes/toluene (15 mL and 5 mL), and diethylzinc (192 μL, 0.168 mmol). Red crystals. Yield = 0.059 g (53%). ^{1}H NMR (C_6D_6, 300 MHz, 25 °C): δ 8.21 (d, J_{HH} = 8.4 Hz, 2H; $C_{10}H$), 7.82 (s overlapping, 2H; C_1H), 7.80 (overlapped m, 4H; $C_{12}H$, $C_{14}H$), 7.32 (s, 2H; C_3H), 7.31 (overlapped m, 2H; C_7H), 7.30 (overlapped m, 2H; C_9H), 7.25 (overlapped m, 4H; $C_{13}H$, $C_{15}H$), 7.02 (overlapped m, 2H; C_8H), 6.84 (tt, J = 1.73, 6.76 Hz, 2H; $C_{16}H$), 2.40 (s, $C_{16}H$; 6H), 2.38 ppm (s, $C_{15}H$; 6H). ^{13}C{^{1}H} NMR (C_6D_6, 75 MHz, 25 °C): δ 154.4 (C_4), 152.4 (C_{11}), 150.8 (C_{Ar}), 139.7 (C_6), 134.5 (C_{Ar}), 131.7 (C_{Ar}), 131.4 (C_9), 129.9 (C_{13}, C_{15}), 129.3 (C_{Ar}), 127.2 (C_7), 126.9 (C_8-H), 126.0 (C_{Ar}), 125.7 (C_{Ar}), 123.3 (C_{10}), 120.9 (C_{16}), 111.3 (C_1), 106.0 (C_3), 22.9 (C_{17}), 21.5 ppm (C_{18}). UV-Vis (THF): λ (ε) 503 (5 870), 393 (8 340), 365 nm (8 050 M^{-1} cm^{-1}). Anal. Calc. for $C_{42}H_{34}N_4Zn$: C, 76.42; H, 5.19. Found: C, 76.37; H, 5.29.

Crystal structure data for **2-Zn**: X-ray quality crystals were grown from diethylether/hexanes solution at -40 °C. Disordered solvent molecules found within the lattice could not be successfully modeled and the respective electron density was removed using the SQUEEZE protocol[22] with the results appended to the end of the accompanying .cif (see Supporting Information). Crystal structure parameters: $C_{42}H_{34}N_4Zn$ 660.10 g/mol, monoclinic, space group $C2/c$; a = 13.1205(8)Å, b = 20.1914(14) Å, c = 15.6328(10) Å, β = 103.329(3)°, V = 4029.9(5) Å^3; Z = 4, ρ_{calcd} = 1.088 g cm^{-3}; crystal dimensions 0.240 x 0.120 x 0.100 mm; diffractometer Bruker D8 QUEST ECO CMOS; Mo K$_\alpha$ radiation, 150(2) K, θ_{max} = 30.631°; 92012 reflections, 6197 independent (R_{int} = 0.0446), direct methods; absorption coeff (μ = 0.639 mm^{-1}), absorption correction semi-

empirical from equivalents (SADABS); refinement (against F_o^2) with SHELXTL V6.1, 215 parameters, 0 restraints, $R_1 = 0.0388$ ($I > 2\sigma$) and $wR_2 = 0.1334$ (all data), Goof = 0.939, residual electron density 0.442 /−0.793 e Å^{-3}.

3. RESULTS AND DISCUSSION

3.1 Ligand and Complex Synthesis

Using analogous Pd-catalyzed cross-coupling/condensation reactions to those reported for the preparation of 4-amino-2-methylphenanthridine[12b], we were able to access both 2-*tert*-butyl- (**1**) and 2,6-dimethyl (**2**) variants of 4-aminophenanthridine suitable for elaboration to our target secondary amine proligands (Scheme 1). Subsequently employing cross-coupling conditions reported for the preparation of 8-(*N*-(3,5-dimethylphenyl)amino)quinoline[17] gave only limited (20%) conversion to **L1**. More forcing conditions (bath temperature 155 ºC; sealed, thick-walled flask; Scheme 1) significantly increased conversion, however, and both ligands could be isolated in high yields after 24 h (**L1**: 80%; **L2**: 84%). 4-aminophenanthridines are apparently not as reactive under Buchwald-Hartwig amination conditions as the smaller 8-aminoquionlines[12b]. Increasing reaction times to 42 h did not appreciably improve yields; however, using a slight excess of the respective aminophenanthridine (1.1 equiv.) did boost conversions above 95%, with a concomitant increase in the isolated yield of proligands.

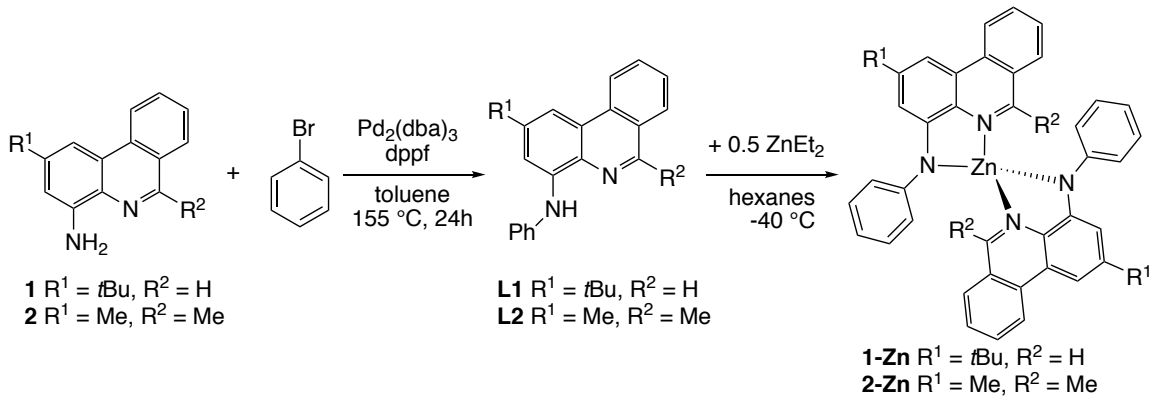

1 R^1 = *t*Bu, R^2 = H
2 R^1 = Me, R^2 = Me

L1 R^1 = *t*Bu, R^2 = H
L2 R^1 = Me, R^2 = Me

1-Zn R^1 = *t*Bu, R^2 = H
2-Zn R^1 = Me, R^2 = Me

Scheme 1. Synthesis of ligands **L1-L2** and complexes **1-Zn/2-Zn**.

With the proligands in hand, zincation was pursued using a similar strategy to the preparation of **Zn(^{q}NN^{SiMe3})$_2$**[11]. Addition of 0.5 equivalents of diethylzinc in hexanes at -40 °C drop-wise to solutions of the respective proligands led to immediate colour change from yellow to deep red-pink. Complexes **1-Zn** and **2-Zn** could be isolated following recrystallization at low temperature as deep red solids. Both Zn complexes are highly soluble in organic solvents including diethylether and toluene, precipitating from hexanes only at low temperature. While both complexes are stable in solution and the solid-state in the absence of air or moisture, the complexes readily engage in transamination reactions when provided with a proton source (e.g., H_2O), returning the protonated proligands as the major organic product.

In solution, multi-nuclear NMR data is consistent with deprotonation and coordination of the proligands to the metal. The resonance attributed to the exchangeable amine proton (N*H*: **L1** 8.29; **L2** 8.38 ppm) is lost, with the remaining aryl and phenanthridine C*H* resonances shifting upon coordination to the metal. Sharp signals for all protons are observed at room temperature, consistent with a single isomer in solution

under these conditions, with no evidence of monomer-dimer equilibrium. Interestingly, in **1-Zn**, the hydrogen nucleus in the C_6 position in the phenanthridinyl moiety adjacent to the coordinated nitrogen is observed at 8.25 ppm. This is significantly upfield of the signal for this same hydrogen in the proligand **L1** (9.13 ppm). A downfield shift of the ^{1}H resonance attributed to the [C*H*] unit in the 6-position is typical of phenanthridine derivatives[12], consistent with a dominant 'imine-bridged, biphenyl' resonance contributor that maximizes the number of aromatic subunits in accordance with Clar's postulate[35]. We previously observed that coordination of phenathrindine-containing amido pincer-type ligands to Group 10 metal ions results a metal-dependent shift of the [C_6*H*] resonance, with binding to Ni(II) inducing an upfield shift, Pt(II) a downfield shift, and Pd(II) a less pronounced downfield shift in square-planar environments[12b].

*3.2 Solid-State Structures of **1-Zn** and **2-Zn***

Elemental analysis of the deep red solids was consistent with the formulation of **1-Zn** and **2-Zn** as 2:1 ligand-metal complexes. To establish nuclearity in the solid-state, we turned to single crystal X-ray diffraction (Figure 2). This allowed examination of the coordination geometry of the metal centres and in turn enabled rationalization of observations such as the higher field resonance of the C_6*H* discussed above. Deep red crystals of **1-Zn** and **2-Zn** suitable for diffraction experiments were grown by diffusion of hexane vapors into diethylether solutions at -40 ºC. In the structures of both complexes, the Zn(II) centres are monomeric and four-coordinate, with each metal coordinated by two equivalents of ligand. Calculated τ_δ indices[36] are consistent with geometries significantly

distorted from ideal tetrahedral: distorted sawhorse for **1-Zn** (τ_δ = 0.59) and distorted tetrahedral for **2-Zn** (τ_δ = 0.64; Table 1). In comparison, **Zn(${}^{q}NN^{SiMe3}$)$_2$** has a similar distorted tetrahedral geometry to **2-Zn** (τ_δ ~ 0.63-0.65)[11] while the pared down **Zn(${}^{q}NN^{H}$)$_2$** (τ_δ ~ 0.56) is closer to the distorted sawhorse geometry of **1-Zn**. As introduction of a methyl substituent to the C_6 position should increase the steric bulk of **L2** compared with **L1** closer to the metal, the trend in geometry of **2-Zn** vs **1-Zn** might be expected to mirror that of **Zn(${}^{q}NN^{SiMe3}$)$_2$** vs **Zn(${}^{q}NN^{H}$)$_2$**. As the bite angles of the four ligands are all similar, the origin of the structural differences appears rooted in the interligand angles. For **Zn(${}^{q}NN^{SiMe3}$)$_2$** vs **Zn(${}^{q}NN^{H}$)$_2$**, the added bulk at the amido nitrogens results in greater interligand repulsion; for **1-Zn** and **2-Zn**, methylation *ortho* to the phenanthridine nitrogen opens up interligand angles involving the heterocyclic donor. The geometry of the amido nitrogen atom is nearly perfectly planar in all four complexes, reflecting sp^2 hybridization typical of zinc amides[37], with the sum of bond angles ~ 360° despite the lack of metal(d)-N(p) π interactions.

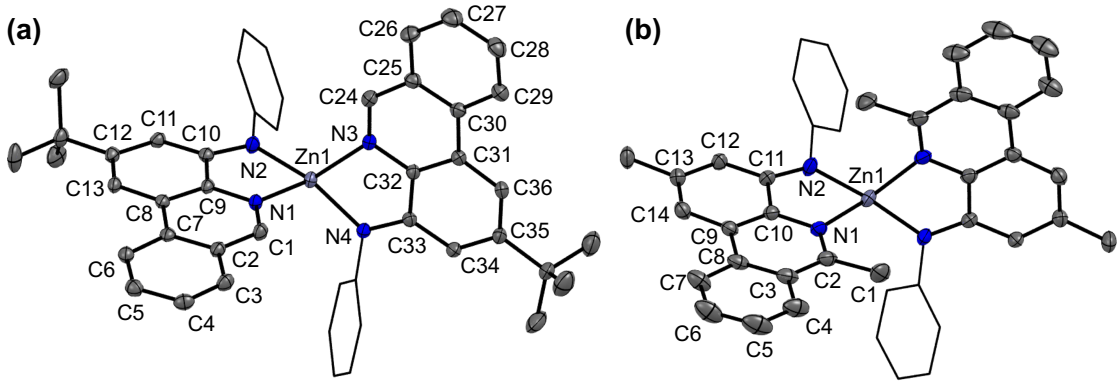

Figure 2. ORTEPs[38] of (a) **1-Zn** and (b) **2-Zn** with thermal ellipsoids shown at 50% probability levels. Hydrogen atoms, co-crystallized solvent molecules (**1-Zn**), symmetry-generated atom labels and other selected atom labels omitted for clarity.

The lower τ_5 values for **1-Zn** and **Zn(${}^{q}NN^{H}$)$_2$** which present comparably *less* steric bulk than **2-Zn** and **Zn(${}^{q}NN^{H}$)$_2$**, respectively, are interesting in light of the assumption that, given the absence of ligand field effects, d^{10} Zn(II) ions would be expected to favor more tetrahedral-like geometries[37]. DFT optimization with implicit solvation (THF) resulted in further distortion of the geometries of the zinc complexes with τ_5 of 0.44 (sawhorse) and 0.57 (distorted sawhorse) for **1-Zn** and **2-Zn** (Table S3), respectively. In this case, therefore, the constraints of ligand geometry appear to enforce distorted sawhorse geometries, which are perturbed toward distorted tetrahedral geometries by increased ligand bulk. With respect to the unanticipated upfield shift of the C_6H resonance in **1-Zn**, the distortion away from tetrahedral likely increases the shielding of the H nucleus in this position, resulting in a relatively upfield resonance.

Table 1. Selected structural parameters for **1-Zn** and **2-Zn** and related compounds.[a]

	1-Zn	**2-Zn**	**Zn(${}^{q}NN^{SiMe3}$)$_2$**[11]	**Zn(${}^{q}NN^{H}$)$_2$**[5a]
Zn-N^{hetero}	2.0598(17), 2.0618(17)	2.0561(13)	2.069, 2.070	2.081(1)
Zn-N^{amido}	1.9455(17), 1.9520(17)	1.9400(12)	1.940, 1.946	1.919(2)
Intraligand N-Zn-N (bite angle)	82.72(7), 83.57(7)	83.78(5)	84.41, 84.56	83.34(6)
Interligand N^{hetero}-Zn-N^{hetero}	109.90(7)	112.96(7)	115.00, 115.45	109.89(7)
Interligand N^{amido}-Zn-N^{amido}	141.49(8)	137.08(8)	136.25, 137.84	145.46(9)

Interligand N^{amido}-Zn-N^{hetero}	123.69(7), 115.51	120.82(5)	119.68, 118.79	117.20(6)
Σ(angles at N^{amido})	360, 359	357	360, 360	360
τ_δ[36]	0.59	0.64	0.63, 0.65	0.56
Geometry[36]	distorted sawhorse	distorted tetrahedral	distorted tetrahedral	distorted sawhorse

[a] Values for all crystallographically distinct molecules, with standard uncertainties listed when available. Data for **Zn(${}^{q}NN^{SiMe3}$)$_2$**[11] **Zn(${}^{q}NN^{H}$)$_2$**[5a] are from the appropriate references.

3.3 Electronic Structure and Physical Property Studies

Absorbance spectra were collected for solutions of both proligands and their corresponding Zn complexes. UV-Vis spectra of **L1** and **L2** reveal a small hypsochromic shift (14 nm) in the lowest energy band upon methylation of the C_6 position and replacement of the *t*Bu substituent with a methyl substituent (Figure 3). Time dependent DFT (TD-DFT) reproduces this trend, and assigns these transitions as HOMO→LUMO in character for both proligands (see Supporting Information, Table S1). Orbital analysis reveals the HOMO consists of contributions from the N_{amido} lone pair, filled phenyl π orbitals and C_1-$C_{4a/b}$ fragment of phenanthridine, while the LUMO is comprised of vacant π* orbitals localized on phenanthridine, identifying these transitions as (*n*+π)→π* (Table S4 and S5). Absorption features between 325-375 nm are not as affected by ligand substitution and are assigned as (n+π)→π* (HOMO→LUMO+1; Table S1). Comparison of orbital energies (Figure S20) suggests the blue shift of λ_{max} arises from destabilization of the LUMO of **L2** with methylation at C_6; the HOMO and the LUMO+1 of **L1** and **L2** are nearly degenerate, and are effectively unaffected by methylation at C_6 as these MOs do not have lobes located at the C_6=N sub-unit of phenanthridine.

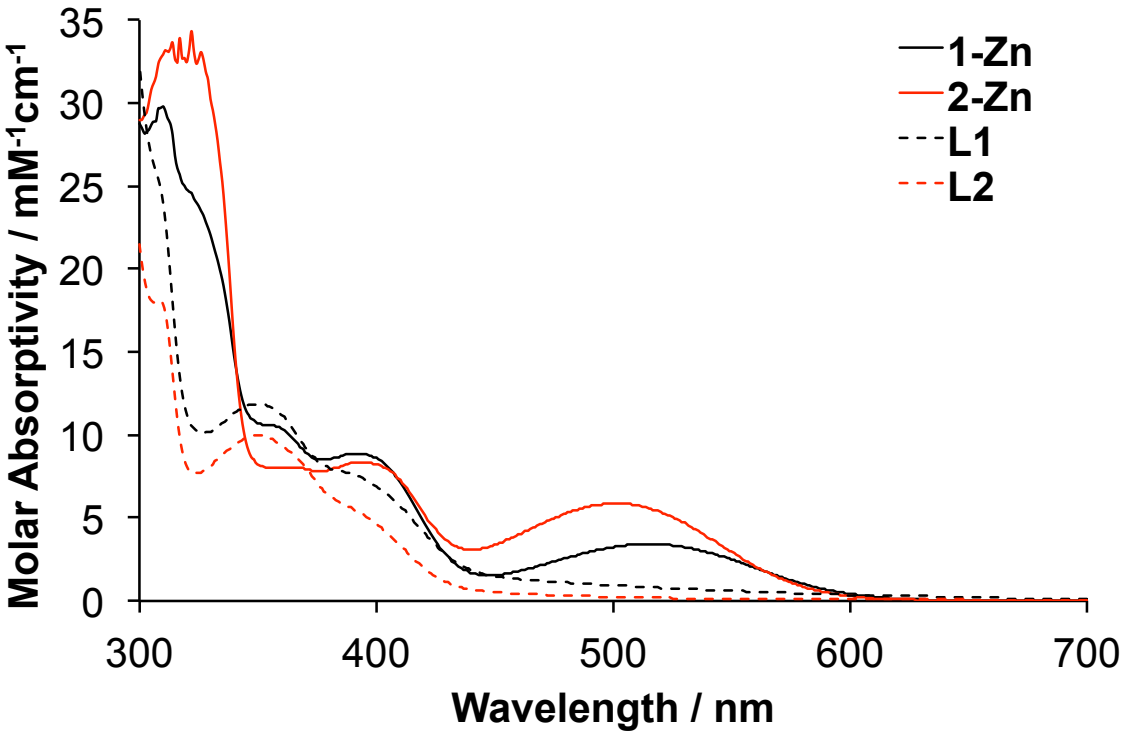

Figure 3. UV-Vis absorption spectra collected in THF at 25 °C for **L1** and **L2** (10 μM), **1-Zn** (154 μM) and **2-Zn** (144 μM).

Consistent with the deep red colour of the zinc complexes, a broad, low energy band (450-700 nm) is observed for both **1-Zn** and **2-Zn**, with a similar hypsochromic shift in the band maximum for the latter compound, also reproduced by TD-DFT (Table S1). This is again attributed to methylation at the C_6-position destabilizing the LUMO (Table S5), comprised of π* orbitals localized at the phenanthridine C_6=N sub-unit (Figure 4).

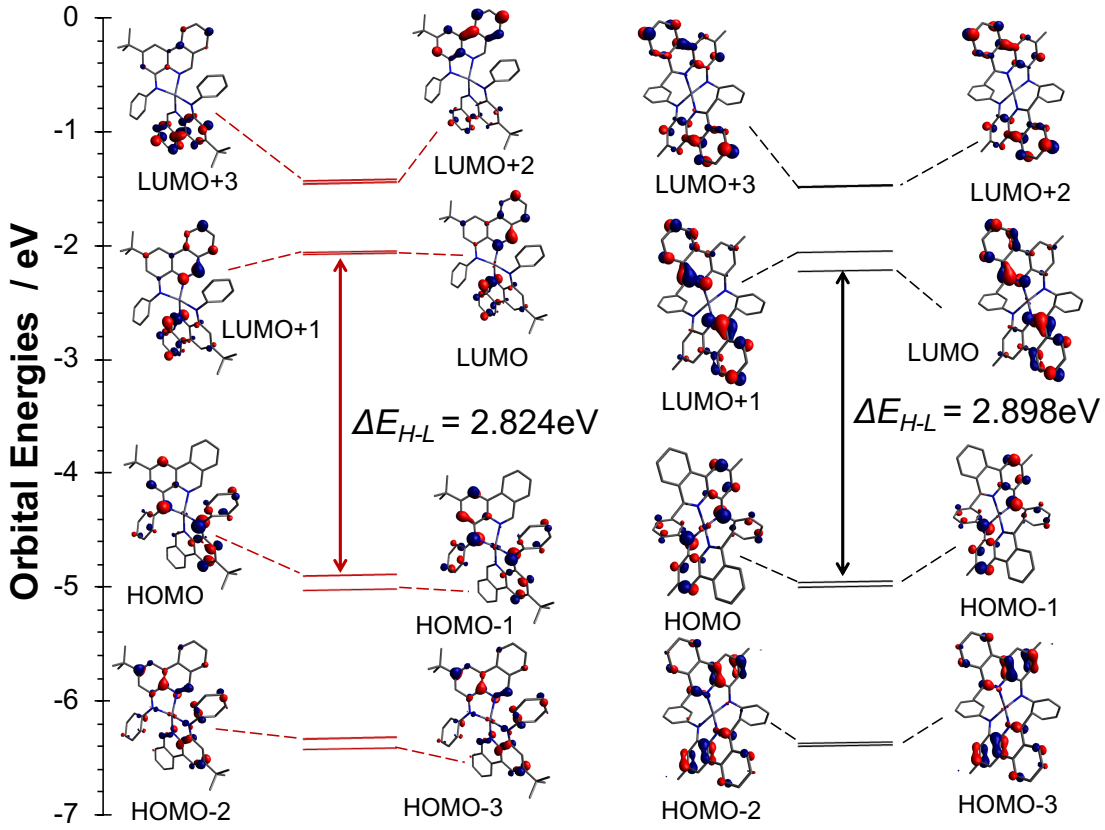

Figure 4. TD-DFT energies and orbital diagrams for the highest four occupied and lowest four unoccupied MOs of **1-Zn** and **2-Zn**.

Electrochemical analysis (Table 2, Figure 5) reveals that the first oxidation events for **1-Zn** and **2-Zn** occur at very similar potentials, consistent with similar energies for their HOMOs. The reversibility of this oxidation event is somewhat dependent on the ligand substitution pattern; methylation at the C_6 position appears to stabilize the one-electron oxidized species [**2-Zn**]$^+$ on the electrochemical timescale; we were unsuccessful at isolating the analogous chemically oxidized species.

For both complexes, TD-DFT calculates the lowest energy absorption band to be comprised of two transitions with significant oscillator strength and similar energies (Table

S1). The lower energy of these is a HOMO→LUMO transition, with a small contribution from HOMO→LUMO+1, while the slightly higher energy transition is HOMO-1→LUMO+1 in character for **1-Zn**, and split evenly between HOMO→LUMO+1/HOMO-1→LUMO for **2-Zn**. The frontier orbitals of **1-Zn** and **2-Zn** bear close resemblance to those of the proligands (Figure S20). The composition of these orbitals allows assignment of interligand charge transfer character (LLCT) to the lowest energy band (Table S6 and S7).

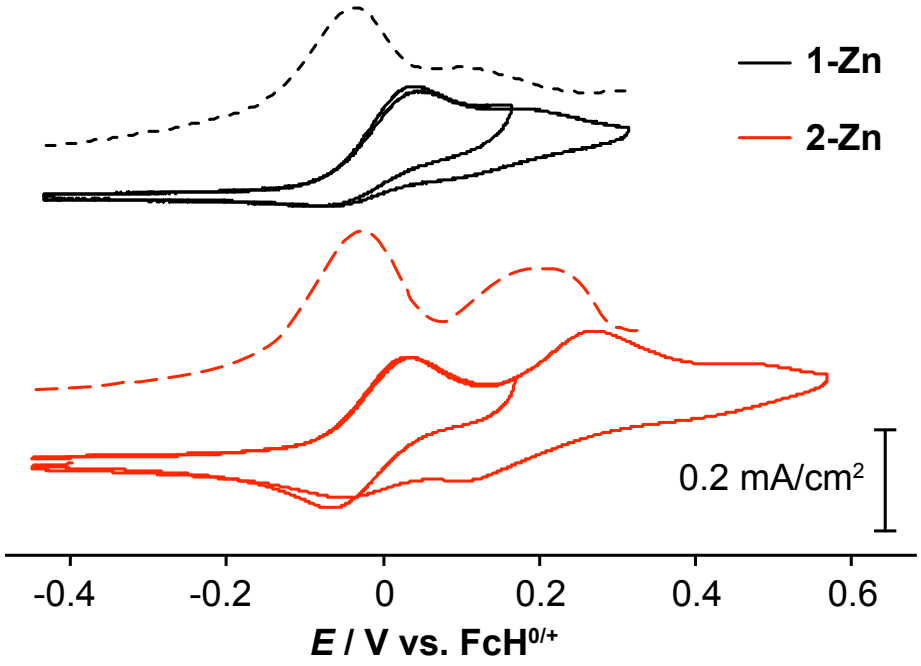

Figure 5. Cyclic voltammograms (—) and corresponding differential pulse voltammograms (---) of **1-Zn** (0.9 mM) and **2-Zn** (1.1 mM) in CH_2Cl_2 at 22 °C, scan rate of 100 mV/s, with 0.1 M nBu$_4$NPF$_6$ as supporting electrolyte.

The charge-transfer character assignment is consistent with the negative solvatochromism observed in Figure S15-S16 (red-shifting of the lowest energy band with decreasing solvent polarity)[39]. In comparison, the position of the middle energy band

(375-425 nm) observed for **1-Zn** and **2-Zn** is unperturbed relative to the lowest energy band. TD-DFT analysis reveals this band is dominated by a single transition, involving multiple components that are also interligand (n+π)-π*, involving the filled phenyl π orbital and the C_1-$C_{4a/b}$ sub-unit of phenanthridine, but with less spatial separation of charge upon excitation, and hence likely a lower response to changes in solvent polarity.

Table 2. Electrochemistry, UV-Vis and emission data for all complexes.

	$E_{1/2}$/V[a]	Δ_{ptp}/ mV[a]	i_{red}/i_{ox}[b]	λ/nm (ε/$M^{-1}cm^{-1}$)	Emission[c] λ/nm	Φ_F x 10^2 [d]
L1	0.45, 0.86	309	0.036	405 (sh), 355 (11 710), 309 (sh)	455	4.7
L2	0.39, 0.82	296	0.022	402 (sh), 350 (10 000), 310 (17 870)	--	--
1-Zn	-0.036, 0.10	96, 105	0.81, 1.1	515 (3 430), 392 (8 890), 362 (10 900), 328 (sh)	455	0.94
2-Zn	-0.035, 0.21	93, 182	0.75, 0.77	503 (5 870), 393 (8 340), 365 (8 050)	--	--

[a] vs. $FcH^{0/+}$. Peak-to-peak separation of a given redox couple. Recorded at scan rates of υ = 100 mV/s.

[b] Ratio of cathodic to anodic currents for a given redox couple. Recorded at scan rates of υ = 100 mV/s and determined from CVs of isolated peaks.

[c] in THF, 22 °C, λ_{ex} = 366 nm.

[d] Relative to quinine sulfate.

As expected for phenanthridine-based materials[40], **L1** is emissive in solution (Figure 6). There is no appreciable emission, however, from **L2**, apparently a result of C_6 methylation. Upon complexation, the Zn(II) complexes were not emissive when excited from the lowest absorption band. Excitation into the middle absorption band results in

emission from **1-Zn**, although the intensity of emission is considerably weaker than from **L1**. As similar quantum yields are measured from **L1** in neutral and acidic solution (i.e., from [**L1**-H]$^{+}$) emission quenching is not considered to result from nitrogen lone pair donation to a Lewis acid (i.e., Zn^{2+} or H^{+}). Rather, quenching is likely due to overlap of ligand-based emission peaks with the lowest absorption band resulting in intermolecular energy transfer[41]. Aggregate-induced emission from **1-Zn** and **2-Zn** was also explored (Figures S15-S16); only a minimal increase in emission peak area for the Zn(II) complexes was observed.

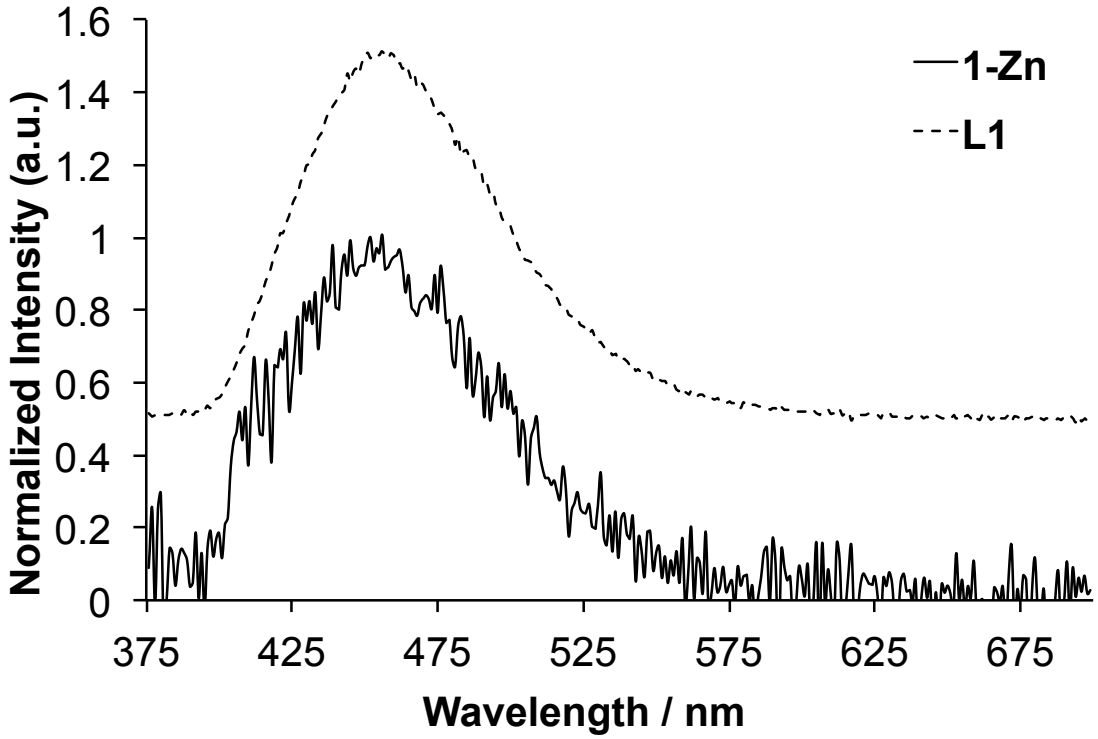

Figure 6. Emission spectra of **L1** and **1-Zn** in THF at 25 °C (λ_{ex} = 366 nm).

4. CONCLUSION

Two novel heteroleptic, chelating proligands based on (4-amino)phenanthridines (**L1** and **L2**) bearing a luminescent and electrochemically active phenanthridinyl unit have been prepared and used to support mononuclear amide complexes of zinc. X-ray structural analysis confirms the mononuclearity of the Zn amide complexes, and reveals that substitution of the benzannulated ligand adjacent to the coordinating nitrogen leads to further distortion from tetrahedral to distorted sawhorse type geometry. Cyclic voltammograms show quasi-reversible and irreversible oxidations, assigned to the amido lone pair. The reversibility of the oxidation events on the electrochemical time scale appears to be controlled to some extent by the ligand substitution pattern. Both **L1** and **1-Zn** are emissive in CH_2Cl_2 solution, while C_6 methylation largely quenches emission from **L2** and **2-Zn**, suggesting that luminescent materials derived from this ligand design should avoid substitution at this position. Stabilization of emissive states and alternative complex oxidation states through ligand design along with reactivity studies are currently underway.

ACKNOWLEDGEMENTS

The following sources are gratefully acknowledged: Natural Sciences Engineering Research Council of Canada for a Discovery Grant to DEH (RGPIN-2014-03733) and a USRA award to TM; the Canadian Foundation for Innovation and Research Manitoba for an award in support of an X-ray diffractometer (CFI #32146); the University of Manitoba for GETS support (IBML). Prof. Song Liu is gratefully acknowledged for access to a CHNS Analyzer, and Jason D. Braun is thanked for collecting elemental analysis data for **1-Zn** and **2-Zn**. Prof. Mazdak Khajepour and Dr. Carl Bartels are thanked for access to

spectrophotometers, and Dr. Rebecca L. Davis is thanked for helpful discussions regarding computation.

Appendix A. Supplementary Material

CCDC 1868447-1868448 contains the supplementary crystallographic data for **1-Zn** and **2-Zn**. These data can be obtained free of charge via http://www.ccdc.cam.ac.uk/conts/retrieving.html, or from the Cambridge Crystallographic Data Centre, 12 Union Road, Cambridge CB2 1EZ, UK; fax: (+44) 1223-336-033; or e-mail: deposit@ccdc.cam.ac.uk. Supporting Information associated with this article containing NMR spectra, electrochemical analysis data for **L1** and **L2**, and full computational details, as well as a combined CIF for **1-Zn** and **2-Zn**, is available in the online version at http://dx.doi.org/ XX.XXX/XXXXX.

REFERENCES

[1] E. Frankland, Proc. R. Soc. 8 (1857) 502-506.
[2] (a) J. M. Bakker, G. B. Deacon, P. C. Junk, G. J. Moxey, D. R. Turner, Z. Anorg. Allg. Chem. 633 (2007) 251-255; (b) J. Chyba, Z. Moravec, M. Necas, S. Mathur, J. Pinkas, J. Organomet. Chem. 749 (2014) 197-203.
[3] R. E. Mulvey, Chem. Commun. (2001) 1049-1056.
[4] D. R. Armstrong, G. C. Forbes, R. E. Mulvey, W. Clegg, D. M. Tooke, J. Chem. Soc., Dalton Trans. (2002) 1656-1661.
[5] (a) A. Malassa, C. Koch, B. Stein-Schaller, H. Goerls, M. Friedrich, M. Westerhausen, Inorg. Chim. Acta 361 (2008) 1405-1414; (b) J. J. Sandoval, E. Alvarez, P. Palma, A. Rodriguez-Delgado, J. Campora, Organometallics 37 (2018) 1734-1744.
[6] (a) K. R. K. Prasad, N. N. Joshi, J. Org. Chem. 62 (1997) 3770-3771; (b) K. Soai, T. Shibata In *Organozinc Reagents*; Knochel, P., Jones, P., Eds.; Oxford University Pres: Oxford, UK, 1999, p 245-261.
[7] C. C. Roberts, B. R. Barnett, D. B. Green, J. M. Fritsch, Organometallics 31 (2012) 4133-4141.

[8] (a) O. Just, W. S. Rees, Jr., Adv. Mater. Opt. Electr. 10 (2000) 213-221; (b) E. Maile, R. A. Fischer, Chem. Vap. Deposition 11 (2005) 409-414.
[9] D. A. Gaul, O. Just, W. S. Rees, Jr., Inorg. Chem. 39 (2000) 5648-5654.
[10] H. Schumann, J. Gottfriedsen, F. Girgsdies, Z. Anorg. Allg. Chem. 623 (1997) 1881-1884.
[11] L. M. Engelhardt, P. C. Junk, W. C. Patalinghug, R. E. Sue, C. L. Raston, B. W. Skelton, A. H. White, J. Chem. Soc., Chem. Commun. (1991) 930-932.
[12] (a) R. Mondal, P. K. Giesbrecht, D. E. Herbert, Polyhedron 108 (2016) 156-162; (b) P. Mandapati, P. K. Giesbrecht, R. L. Davis, D. E. Herbert, Inorg. Chem. 56 (2017) 3674-3685; (c) R. Mondal, I. B. Lozada, R. L. Davis, J. A. G. Williams, D. E. Herbert, Inorg. Chem. 57 (2018) 4966-4978.
[13] A. Fukase, J. Kido, Jpn. J. Appl. Phys., Part 2 41 (2002) L334-L336.
[14] J. Kido, J. Endo, Chem. Lett. (1997) 593-594.
[15] J.-M. Valk, T. D. W. Claridge, J. M. Brown, D. Hibbs, M. B. Hursthouse, Tetrahedron: Asymmetry 6 (1995) 2597-2610.
[16] L. Raszeja, A. Maghnouj, S. Hahn, N. Metzler-Nolte, ChemBioChem 12 (2011) 371-376.
[17] J. C. Peters, S. B. Harkins, S. D. Brown, M. W. Day, Inorg. Chem. 40 (2001) 5083-5091.
[18] G. R. Fulmer, A. J. M. Miller, N. H. Sherden, H. E. Gottlieb, A. Nudelman, B. M. Stoltz, J. E. Bercaw, K. I. Goldberg, Organometallics 29 (2010) 2176-2179.
[19] N. G. Connelly, W. E. Geiger, Chem. Rev. 96 (1996) 877-910.
[20] Bruker-AXS, *APEX3 v2016.1-0*,
[21] G. M. Sheldrick, Acta Cryst. A64 (2008) 112-122.
[22] A. L. Spek, Acta Cryst. D65 (2009) 148-155.
[23] A. M. Brouwer, Pure Appl. Chem. 83 (2011) 2213-2228.
[24] M. J. Frisch, G. W. Trucks, H. B. Schlegel, G. E. Scuseria, M. A. Robb, J. R. Cheeseman, G. Scalmani, V. Barone, G. A. Petersson, H. Nakatsuji, X. Li, M. Caricato, A. V. Marenich, J. Bloino, B. G. Janesko, R. Gomperts, B. Mennucci, H. P. Hratchian, J. V. Ortiz, A. F. Izmaylov, J. L. Sonnenberg, D. Williams-Young, F. Ding, F. Lipparini, F. Egidi, J. Goings, B. Peng, A. Petrone, T. Henderson, D. Ranasinghe, V. G. Zakrzewski, J. Gao, N. Rega, G. Zheng, W. Liang, M. Hada, M. Ehara, K. Toyota, R. Fukuda, J. Hasegawa, M. Ishida, T. Nakajima, Y. Honda, O. Kitao, H. Nakai, T. Vreven, K. Throssell, J. A. Montgomery, J. E. Peralta, F. Ogliaro, M. J. Bearpark, J. J. Heyd, E. N. Brothers, K. N. Kudin, V. N. Staroverov, T. A. Keith, R. Kobayashi, J. Normand, K. Raghavachari, A. P. Rendell, J. C. Burant, S. S. Iyengar, J. Tomasi, M. Cossi, J. M. Millam, M. Klene, C. Adamo, R. Cammi, J. W. Ochterski, R. L. Martin, K. Morokuma, O. Farkas, J. B. Foresman, D. J. Fox, *Gaussian 16, Revision B.01*.
[25] G. Scalmani, M. J. Frisch, J. Chem. Phys. 132 (2010) 114110/114111-114110/114115.
[26] M. D. Hanwell, D. E. Curtis, D. C. Lonie, T. Vandermeersch, E. Zurek, G. R. Hutchison, J. Cheminf. 4 (2012) 17.
[27] H. S. Yu, X. He, D. G. Truhlar, J. Chem. Theory Comput. 12 (2016) 1280-1293.
[28] (a) F. Weigend, R. Ahlrichs, Phys. Chem. Chem. Phys. 7 (2005) 3297-3305; (b) F. Weigend, Phys. Chem. Chem. Phys. 8 (2006) 1057-1065.

[29] M. Dolg, U. Wedig, H. Stoll, H. Preuss, J. Chem. Phys. 86 (1987) 866-872.
[30] (a) C. Lee, W. Yang, R. G. Parr, Phys. Rev. B: Condens. Matter 37 (1988) 785-789; (b) A. D. Becke, J. Chem. Phys. 98 (1993) 1372-1377; (c) A. D. Becke, J. Chem. Phys. 98 (1993) 5648-5652.
[31] (a) D. Feller, J. Comput. Chem. 17 (1996) 1571-1586; (b) K. L. Schuchardt, B. T. Didier, T. Elsethagen, L. Sun, V. Gurumoorthi, J. Chase, J. Li, T. L. Windus, J. Chem. Inf. Model. 47 (2007) 1045-1052.
[32] D. Rappoport, F. Furche, J. Chem. Phys. 133 (2010) 134105/134101-134105/134111.
[33] N. M. O'Boyle, A. L. Tenderholt, K. M. Langner, J. Comput. Chem. 29 (2008) 839-845.
[34] A. L. Tenderholt, *QMForge: A Program to Analyze Quantum Chemistry Calculations*, version 2.4, https://qmforge.net.
[35] Z. B. Maksić, D. Barić, T. Müller, J. Phys. Chem. A 110 (2006) 10135-10147.
[36] M. H. Reineke, M. D. Sampson, A. L. Rheingold, C. P. Kubiak, Inorg. Chem. 54 (2015) 3211-3217.
[37] J. T. Jastrzebski, J. Boersma, G. Koten In *PATAI'S Chemistry of Functional Groups*; Rappoport, Z., Ed. 2009.
[38] C. F. Macrae, P. R. Edgington, P. McCabe, E. Pidcock, G. P. Shields, R. Taylor, M. Towler, J. van de Streek, J. Appl. Cryst. 39 (2006) 453-457.
[39] C. Reichardt, Chem. Rev. 94 (1994) 2319-2358.
[40] L.-M. Tumir, M. R. Stojkovic, I. Piantanida, Beilstein J. Org. Chem. 10 (2014) 2930-2954, 2925 pp.
[41] A. J. Howarth, M. B. Majewski, M. O. Wolf, Coord. Chem. Rev. 282-283 (2015) 139-149.